ELSEVIER

Journal of Neuroscience Methods 122 (2003) 123–140

JOURNAL OF NEUROSCIENCE METHODS

www.elsevier.com/locate/jneumeth

Closed-loop multivariable system identification for the characterization of the dynamic arm compliance using continuous force disturbances: a model study

Erwin de Vlugt *, Alfred C. Schouten, Frans C.T. van der Helm

Man Machine Systems and Control, Department of Design, Engineering and Production, Delft University of Technology, Mekelweg 2, 2628 CD, Delft, The Netherlands

Received 26 April 2002; received in revised form 17 September 2002; accepted 18 September 2002

Abstract

This study presents a new multivariable closed-loop identification technique for estimating the dynamic compliance of the multijoint human arm during posture maintenance. The method is designed for the application of continuous force disturbances that facilitate interaction of the limb with the environment. The dynamic compliance of the arm arises from different physiological mechanisms and is important for maintaining stable postures and to suppress disturbances. Estimates can be useful to analyze the ability of the nervous system to adapt the arm compliance to different types of disturbances and environments. The technique is linear and requires no a priori knowledge of the system. Linear system behavior is justified for posture tasks where the hand position deviates slightly from a reference position. Interaction results in a closed-loop configuration of arm and environment. The problem with previous methods is the restriction to open-loop systems. With the current technique, the dynamic arm compliance is separately estimated from the closed-loop. The accuracy of the identification technique is tested by simulations for different values of the dynamic compliance of the arm and environment and for different methodological parameters. It is concluded that the identification technique is accurate, even for short observation periods and severe noise.

Keywords: Closed-loop identification; Environments; Dynamic compliance; Frequency domain; Force disturbance; Deterministic signals

1. Introduction

Human arm posture maintenance is the result of coordinated forces around the joints at particular joint angles. The goal of posture control is to maintain a certain mean position and to minimize deviations in the presence of force disturbances. With respect to the displacements, the restoring forces result from elastic, viscous and inertial properties. Elastic and viscous properties of a limb can be adapted and originate from intrinsic muscle stiffness and damping and additionally from reflexive feedback from muscle spindles (Toft et al., 1991; Doemges and Rack, 1992a; Kirsch et al., 1993; Kearney et al., 1997). Both intrinsic and reflexive contributions depend on (a) the task instruction given to the subjects (Smeets and Erkelens, 1991; Doemges and Rack, 1992b; Gomi and Osu, 1998), (b) the properties and type of the disturbance signal (Stein and Kearney, 1995; Cathers et al., 1999; Van der Helm et al., 2002), (c) the configuration, of the arm (Mussa-Ivaldi et al., 1985; Dolan et al., 1993) and (d) the mechanical properties of the environment (Milner and Cloutier, 1993; De Vlugt et al., 2002).

Most of these studies used transient position disturbances to identify only the stiffness of single joints and some have retrieved stiffness ellipses for the two-joint case (Mussa-Ivaldi et al., 1985; Dolan et al., 1993; Gomi and Kawato, 1996). Since position is imposed, the reaction force was taken as the free output variable. The task instruction is mostly formulated so as to maintain a certain force level in certain directions. Other studies analyzed the transient response in EMG signals to separate the reflexive contributions by isolating the

* Corresponding author. Tel.: +31-15-278-5247; fax: +31-15-278-4717.
E-mail address: e.devlugt@wbmt.tudelft.nl (E. de Vlugt).

0165-0270/02/$ - see front matter
PII: S0165-0270(02)00303-5

delayed response from the instantaneous. Only the first hundreds of milliseconds were analyzed where voluntary reactions are likely not to take place (Toft et al., 1991; Stein and Kearney, 1995). A few studies applied continuous stochastic position disturbances to determine the mechanical properties of the limb (Kirsch et al., 1993; Kearney et al., 1997; Cathers et al., 1999; Perreault et al., 2001; Zhang and Rymer, 1997). Compared with transient disturbances, this method allows a faster and more accurate quantification of limb stiffness, damping and mass because a richer frequency range is applied.

However, since position is simply imposed by a manipulator that is assigned a stiffness much larger than that of the concerned limb, the 'responding' forces can by no means change the limb position or muscle lengths. For (ideal) position disturbances, position and force are fully decoupled and there is no matter of active stabilization, i.e. the position servo provides inherent stability. Because of the decoupling, the system can be regarded as an open-loop, facilitating straight forward open-loop identification techniques (Bendat and Piersol, 1986; Ljung, 1999).

In contrast to position disturbances, force disturbances facilitates a functional dynamic analysis of the limb compliance during natural interaction with the environment. Deviations of the endpoint position, as a result of the force disturbance, are determined by the dynamic compliance of both the arm and environment. Efforts of the central nervous system (CNS) to preserve stability by adjusting both intrinsic and reflexive properties have a direct effect on the responding limb position. The interacting behavior results in a closed-loop control configuration of limb and environment together. The problem with previous estimation techniques is the restriction to open-loop systems.

The goal of this study is to develop a closed-loop identification technique, which is appropriate for application of continuous force disturbances and interaction with environments during posture control. The technique is nonparametric, meaning that no a priori knowledge of the system is needed. An important requirement is that the system to be estimated is stationary. This means that its properties remain constant over the observed time period. In fact, the interest is in the system response to the continuous force disturbance. Therefore, anticipatory muscle activation which changes the arm compliance (and acts as an additional force input) should be avoided. This is achieved by using random force disturbances such that prediction is likely excluded. If the system is indeed stationary for these types of force disturbances, the arm compliance can only be the result of constant intrinsic muscle properties and peripheral feedback mechanisms.

Kearney and Hunter (1990) already indicated the great usefulness of closed-loop responses since they characterize joint behavior under natural behavioral conditions. They described the basics for the application of closed-loop estimators for single-joint dynamics. In a recent study from our laboratory, this experimental paradigm is applied to quantify the compliance of the shoulder joint (De Vlugt et al., 2002; Van der Helm et al., 2002).

The present study extends the estimation method for single-joint dynamics to a two-input two-output planar case for estimating arm compliance at the point of interaction or endpoint. In this case the hand reaction force acts as the input and the hand position as the output. The application is also suitable for larger input–output systems. The estimated dynamic compliance is expressed in the frequency domain by means of a matrix frequency response function (MFRF).

In addition to the closed-loop estimator, a signal design method is used for the generation of the force disturbance signals. This method produces unpredictable deterministic signals having exact power at specific frequencies. The main advantage of deterministic signals is that their periodicity prevents bias in the estimates, which would otherwise emerge in the case of application of stochastic signals (Schoukens et al., 1993).

The goodness of the estimation method is verified by simulations for different properties of arm and environmental compliance. Various experimental and methodological conditions are simulated and discussed. The results indicate that the endpoint compliance is estimated very accurately, having negligible bias and variance at rather erroneous conditions, reflected by high values of the multiple coherence functions.

2. Closed-loop system description

Any (bio)mechanical system in its complete dimension and normal functioning, is properly described when a driving force is taken at the input and a movement (position or velocity) as the output. Only in this way the system states follow from integration of inputs, and the output is determined as a (linear) combination of the system states. To understand the underlying mechanisms subserving the mechanical response, the system therefore, should be analyzed in its causal dynamic structures wherein it is defined, i.e. as a dynamic compliance (Hogan, 1985). The compliance comprises stiffness, damping and inertia properties, together with feedback loops, and is expressed in meters per Newton (m/N), i.e. the inverse of the mechanical impedance.

Fig. 1 shows schematically a manipulator to realize an environment. The Cartesian components of the signals are defined in the subjects frame having its origin in the right shoulder. To analyze human arm posture control effectively, the influence of the environment should be kept small compared with the arm. This means that the

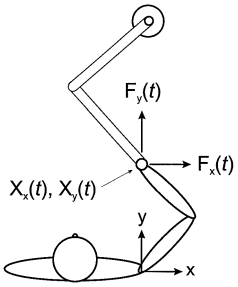

Fig. 1. Schematical configuration of a typical experimental setup to measure the planar dynamic compliance of the human arm. The hand is physically attached to the manipulator. Forces and motions are constrained to a horizontal plane and decomposed in cartesian $(x-y)$ coordinates in the subjects frame. The origin of the frame is usually located in the subject's shoulder rotation center. $\mathbf{F}$ is the (2×1) vector of the hand reaction force and $\mathbf{X}$ is the vector of the endpoint or hand position.

inertia, damping and stiffness of the environment should be as low as possible. Despite lightweight designs and advanced control strategies to increase the apparent (virtual) endpoint compliance, the additional contribution cannot be neglected in practice. Fig. 2 shows the nonlinear blockscheme representing the mechanical interaction of the arm with the environment. The total force acting upon the environment is the summation of an independent external force disturbance $\mathbf{D}(t)$ and the opposing hand reaction force $\mathbf{F}(t)$. The hand force is an internal variable and the hand position $\mathbf{X}(t)$ is the output of the total system. It is assumed that the force disturbance, hand reaction force and hand position are available from measurements.

Fig. 2 can also be interpreted in terms of classical control theory. In that case, the environment represents a mechanical system of which the compliance can be modified by an additional compliance of the human arm, which acts as the dynamic compliance controller.

2.1. Linear closed-loop system description

Most system identification techniques are designed for linear systems, whereas biological systems are highly nonlinear in nature (Winters and Stark, 1985; Kirsch et al., 1994; Stein and Kearney, 1995). To use linear techniques, a nonlinear system should be excited such that it behaves almost linearly. This means that only small variations of system states around a working point are allowed. For human posture maintenance, this requirement is easily met because it is the primary goal of posture control to keep the position deviations small with respect to a reference position. The approximation around a specific reference point will never be perfect. The imperfection of the linearized system with respect to the original nonlinear system is accounted for by an additional residual signal or model remnant $\mathbf{R}(f)$ at the output which is uncorrelated with the input $\mathbf{D}(f)$, see Fig. 3A. The linear dynamic compliance of the human arm is indicated by the MFRF $H_{xf}(f)$. Note that the arm is expressed as the anticausal MFRF $H_{xf}^{-1}(f)$ to preserve the causal definition of the dynamic compliance. The (virtual) compliance of the environment is indicated by the MFRF $E_{xz}(f)$. Any nonlinearities in the virtual compliance are also accounted for by the model remnant $\mathbf{R}(f)$. Volitional force contribution, which is not correlated with the imposed force disturbance $\mathbf{D}(t)$, is represented by the input noise signal $\mathbf{N}(t)$. Finally, measurement noise is indicated by $\mathbf{M}(t)$ and is also assumed uncorrelated with $\mathbf{D}(t)$. Since the control of posture is a disturbance task, the blockscheme of Fig. 3A is redrawn into a disturbance blockscheme (Fig. 3B) with a reference position at the input which has to be maintained. Since model remnant and measurement noise cannot be separated from each other, both noise sources are taken together in one noise source $\mathbf{M}(f)$.

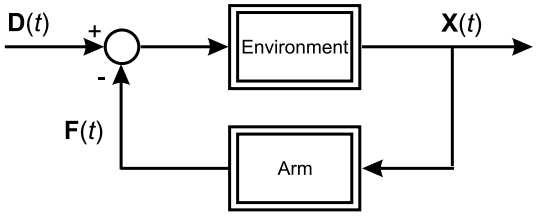

Fig. 2. Basic (nonlinear) closed-loop configuration of the mechanical interaction between the human arm and the manipulator acting as the environment. The total system is excited by a force disturbance $\mathbf{D}(t)$. The force applied by the human arm $\mathbf{F}(t)$ acts in addition, and opposite, to the external force. The system output is the common endpoint or hand position $\mathbf{X}(t)$.

As a result of the closed-loop configuration, the input noise $\mathbf{N}(f)$ also appears in the hand reaction force $\mathbf{F}(f)$ and consequently is correlated with it. It is, therefore, impossible to separate that part in the measured hand position $\mathbf{X}(f)$ that comes from the hand reaction force only. Identification of the arm compliance $H_{xf}(f)$ from $\mathbf{F}(f)$ and $\mathbf{X}(f)$ is, therefore, inadequate. An external signal from outside the loop is needed to eliminate the contribution of the noise source $\mathbf{N}(t)$. The only requirement is that the external signal is uncorrelated with the noise inside the loop. The force disturbance signal $\mathbf{D}(t)$ is taken as the most obvious choice.

The closed-loop estimator of the arm compliance is derived from the system equations in which $\mathbf{F}(t)$ and $\mathbf{X}(t)$ are to be expressed in terms of all the inputs to the closed-loop system, being $\mathbf{D}(t)$, $\mathbf{N}(t)$ and $\mathbf{M}(t)$. First define the frequency transforms of the signals into their $x-y$ components:

$$\mathbf{F}(n\Delta f) = [F_x(n\Delta f) F_y(n\Delta f)]^T$$

$$\mathbf{X}(n\Delta f) = [X_x(n\Delta f) X_y(n\Delta f)]^T$$

$$\mathbf{D}(n\Delta f) = [D_x(n\Delta f) D_y(n\Delta f)]^T$$

$$\mathbf{N}(n\Delta f) = [N_x(n\Delta f) N_y(n\Delta f)]^T$$

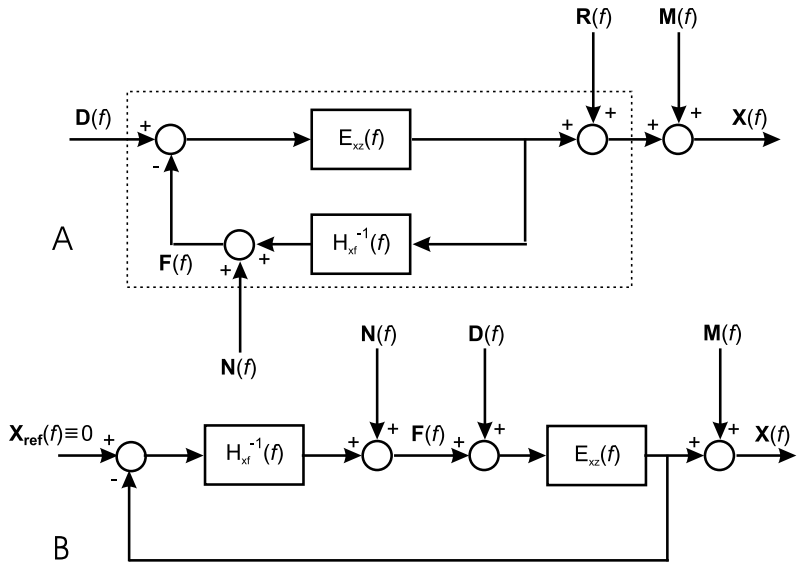

Fig. 3. (A) Linear system approximation of the nonlinear system (dotted box) between input force disturbance $\mathbf{D}(t)$ and output (hand) position $\mathbf{X}(t)$, expressed in the frequency domain. $\mathbf{R}(f)$ is the model remnant, $\mathbf{N}(f)$ system input noise and $\mathbf{M}(f)$ measurement noise. All noise signals are unknown and assumed uncorrelated with $\mathbf{D}(t)$. The dynamic compliance of the arm $H_{xf}(f)$ is configured in a closed-loop with the environmental compliance $E_{xz}(f)$. The arm compliance is presented as its inverse to preserve its causal definition. $\mathbf{F}(f)$ is the hand reaction force, applied via the hand of the subject to the manipulator. (B) Redrawn of A into a disturbance control scheme where the goal is to reduce deviations around a reference position. The posture task is represented by the reference position to be maintained ($\mathbf{X}_{\text{ref}} \equiv 0$) which means that the effect of the force disturbance is to be minimized. The output noise $\mathbf{M}(f)$ also includes the model remnant $\mathbf{R}(f)$.

$$\mathbf{M}(n\Delta f) = [M_x(n\Delta f) M_y(n\Delta f)]^T$$

where T denotes the vector transposed and $n\Delta f$ the discrete frequencies. Hereby, $n \in [0, 1, 2, \ldots, N/2]$, $N = f_s T$, f_s the sample frequency and T the observation time period. The signals are transformed by the standard fast Fourier transform (FFT) algorithm. The system MFRFs $H_{xf}(n\Delta f)$ and $E_{xz}(n\Delta f)$ are defined as two-by-two matrices according to:

$$H_{xf}(n\Delta f) = \begin{bmatrix} H_{x_x f_x}(n\Delta f) & H_{x_x f_y}(n\Delta f) \\ H_{x_y f_x}(n\Delta f) & H_{x_y f_y}(n\Delta f) \end{bmatrix} \quad (1)$$

$$E_{xz}(n\Delta f) = \begin{bmatrix} E_{x_x z_x}(n\Delta f) & E_{x_x z_y}(n\Delta f) \\ E_{x_y z_x}(n\Delta f) & E_{x_y z_y}(n\Delta f) \end{bmatrix} \quad (2)$$

with $z_x = f_x - d_x$ and $z_y = f_y - d_y$. Then the system equations are:

$$\mathbf{F} = [I + H_{xf}^{-1} E_{xz}]^{-1} H_{xf}^{-1} E_{xz} \mathbf{D} + [I + H_{xf}^{-1} E_{xz}]^{-1} \mathbf{N} \quad (3)$$

$$\mathbf{X} = [I + E_{xz} H_{xf}^{-1}]^{-1} E_{xz} \mathbf{D} + [I + E_{xz} H_{xf}^{-1}]^{-1} E_{xz} \mathbf{N} + \mathbf{M} \quad (4)$$

where I is the unit matrix. In Eqs. (3) and (4) the arguments are omitted for readability. Making use of the following algebraic rule:

$$[I + H_{xf}^{-1} E_{xz}]^{-1} H_{xf}^{-1} = H_{xf}^{-1} [I + E_{xz} H_{xf}^{-1}]^{-1}$$

and substituting:

$$L^T = [I + E_{xz} H_{xf}^{-1}]^{-1}$$

into the transposed Eqs. (3) and (4), results in:

$$\mathbf{F}^T = \mathbf{D}^T E_{xz}^T L^T H_{xf}^{-1^T} + \mathbf{N}^T H_{xf}^T L^T H_{xf}^{-1^T} \quad (5)$$

$$\mathbf{X}^T = \mathbf{D}^T E_{xz}^T L^T + \mathbf{N}^T E_{xz}^T L^T + \mathbf{M}^T \quad (6)$$

The cancellation of noise can be established by the use of spectral densities. The spectral densities are obtained by premultiplication of the loop signals (Eqs. (5) and (6)) with the complex conjugate of the external signal $\mathbf{D}(n\Delta f)$ and then taking the expectation value of the products according to:

$$G_{d_i f_j} = E\{\mathbf{D}_i^* \mathbf{F}_j^T\} \quad (7)$$

$$G_{d_i x_j} = E\{\mathbf{D}_i^* \mathbf{X}_j^T\} \quad i, j \in [x, y] \quad (8)$$

where * denotes the complex conjugate, G the spectral density matrix and $E\{\cdot\}$ the expectation operator. Application of spectral densities to the system equations (Eqs. (5) and (6)) gives:

$$G_{df} = G_{dd} E_{xz}^T L^T H_{xf}^{-1^T} + G_{dn} H_{xf}^T L^T H_{xf}^{-1^T} \quad (9)$$

$$G_{dx} = G_{dd} E_{xz}^T L^T + G_{dn} E_{xz}^T L^T + G_{dm} \quad (10)$$

with

$$G_{df} = \begin{bmatrix} G_{d_x f_x} & G_{d_x f_y} \\ G_{d_y f_x} & G_{d_y f_y} \end{bmatrix}, \quad G_{dx} = \begin{bmatrix} G_{d_x x_x} & G_{d_x x_y} \\ G_{d_y x_x} & G_{d_y x_y} \end{bmatrix},$$

$$G_{dd} = \begin{bmatrix} G_{d_x d_x} & G_{d_x d_y} \\ G_{d_y d_x} & G_{d_y d_y} \end{bmatrix}$$

The external force disturbance is assumed uncorrelated

with both noise signals such that G_{dm} and G_{dn} equal the nulmatrix. As a result, the corresponding cross-spectra vanish from Eqs. (9) and (10). The arm compliance follows from multiplication of both cross-spectral densities, according to:

$$G_{df}^{-1}G_{dx} = H_{xf}^{T}L^{-1^T}E_{xz}^{-1^T}G_{dd}^{-1}G_{dd}E_{xz}^{T}L^{T} = H_{xf}^{T} \tag{11}$$

A sufficient requirement for the external force disturbance signals is that the matrix G_{dd} is invertible (Eq. (11)), which means that both signals may not be fully coupled to avoid matrix singularity. This still allows the signals in both directions to be correlated with each other. The closed-loop estimator is, therefore, indifferent to input coupling, which follows directly from Eq. (11) where the product $G_{dd}^{-1}G_{dd}$ vanishes.

The purpose of the closed-loop estimator is to obtain an accurate estimate of the arm compliance H_{xf}.

2.2. Closed-loop system estimation

The derivation of the arm compliance (Eq. (11)) is a theoretical one, based on expectation values in the definition of the spectral densities (Eqs. (7) and (8)). In fact, these definitions only hold for infinitely long observations. A practical approximation of spectral densities, based on finite time records, is obtained by multiplication of the FFT-transformed signals according to:

$$\hat{G}_{d_i f_j} = \mathbf{D}_i\mathbf{F}_j^{*} \approx E\{\mathbf{D}_i\mathbf{F}_j\} = G_{d_i f_j} \quad i,\ j \in [x,\ y] \tag{12}$$

where $\hat{G}$ denotes the estimate of the true spectral density G (Bendat and Piersol, 1986). Applying the approximation also to G_{dx} in Eq. (11) gives the final closed-loop estimator:

$$\hat{H}_{xf} = \hat{G}_{dx}^{T}\hat{G}_{df}^{-1^T} \tag{13}$$

with $\hat{H}_{xf}$ the estimated MFRF of the dynamic arm compliance. Dividing the above equation into the matrix components gives:

$$\hat{H}_{x_x f_x} = \frac{\hat{G}_{d_x x_x}[1 - \hat{G}_{d_y x_x}\hat{G}_{d_x f_y}/\hat{G}_{d_x x_x}\hat{G}_{d_y f_y}]}{\hat{G}_{d_x f_x}[1 - \hat{G}_{d_y f_x}\hat{G}_{d_x f_y}/\hat{G}_{d_x f_x}\hat{G}_{d_y f_y}]} \quad \hat{H}_{x_x f_y} = \frac{\hat{G}_{d_y x_x}[1 - \hat{G}_{d_x x_x}\hat{G}_{d_y f_x}/\hat{G}_{d_y x_x}\hat{G}_{d_x f_x}]}{\hat{G}_{d_y f_y}[1 - \hat{G}_{d_y f_x}\hat{G}_{d_x f_y}/\hat{G}_{d_y f_y}\hat{G}_{d_x f_x}]}$$

$$\hat{H}_{x_y f_x} = \frac{\hat{G}_{d_x x_y}[1 - \hat{G}_{d_y x_y}\hat{G}_{d_x f_y}/\hat{G}_{d_x x_y}\hat{G}_{d_y f_y}]}{\hat{G}_{d_x f_x}[1 - \hat{G}_{d_y f_x}\hat{G}_{d_x f_y}/\hat{G}_{d_x f_x}\hat{G}_{d_y f_y}]} \quad \hat{H}_{x_y f_y} = \frac{\hat{G}_{d_y x_y}[1 - \hat{G}_{d_x x_y}\hat{G}_{d_y f_x}/\hat{G}_{d_y x_y}\hat{G}_{d_x f_x}]}{\hat{G}_{d_y f_y}[1 - \hat{G}_{d_y f_x}\hat{G}_{d_x f_y}/\hat{G}_{d_y f_y}\hat{G}_{d_x f_x}]}$$

The left terms in both numerator and denominator corresponds to the case of no cross coupling between the x and y components in the closed-loop system, i.e. of two decoupled single-input single-output (SISO) systems. The fractions within brackets are corrections for the case of nonzero coupling, i.e. the existence of off-diagonal terms in the MFRFs, which is normally the case in human arm endpoint compliance.

A common indicator of the amount of noise entering the system, are the multiple coherence functions (Bendat and Piersol, 1986):

$$\hat{\gamma}^2_{x_x d_{xy}} = \frac{\hat{P}_{x_x d_x}\hat{G}_{d_x x_x} + \hat{P}_{x_x d_y}\hat{G}_{d_y x_x}}{\hat{G}_{x_x x_x}}$$

$$\hat{\gamma}^2_{x_y d_{xy}} = \frac{\hat{P}_{x_y d_x}\hat{G}_{d_x x_y} + \hat{P}_{x_y d_y}\hat{G}_{d_y x_y}}{\hat{G}_{x_y x_y}} \tag{14}$$

with $\hat{\gamma}^2_{x_x d_{xy}}$ multiple coherence function from both inputs (D_x and D_y) to the output in x-direction (X_x) and $\hat{\gamma}^2_{x_y d_{xy}}$ from both inputs to the output in y-direction (X_y). When both the multiple coherence functions are close to one, the power of any noise is small and the output $\mathbf{X}$ is almost linearly related to the input $\mathbf{D}$. In the case where the multiple coherence functions are close to zero, the power of noise entering the system is large. The multiple coherence functions (Eq. (14)) make use of $\hat{P}_{x_i d_j}$ ($i,\ j \in [x,\ y]$), which is the open-loop estimated MFRF of the complete system from force disturbance to hand position, according to:

$$\hat{P}_{xd} = \hat{G}_{dx}^{T}\hat{G}_{dd}^{-1^T} \tag{15}$$

and specified into its components gives:

$$\hat{P}_{x_i d_x} = \frac{\hat{G}_{d_x x_i}[1 - \hat{G}_{d_x d_y}\hat{G}_{d_y x_i}/\hat{G}_{d_y d_y}\hat{G}_{d_x x_i}]}{\hat{G}_{d_x d_x}[1 - \hat{\gamma}^2_{d_x d_y}]}$$

$$\hat{P}_{x_i d_y} = \frac{\hat{G}_{d_y x_i}[1 - \hat{G}_{d_y d_x}\hat{G}_{d_x x_i}/\hat{G}_{d_x d_x}\hat{G}_{d_y x_i}]}{\hat{G}_{d_y d_y}[1 - \hat{\gamma}^2_{d_x d_y}]} \quad i \in [x,\ y] \tag{16}$$

where $\hat{\gamma}^2_{d_x d_y}$ is the estimated coherence function between both disturbance signals and defined as:

$$\hat{\gamma}^2_{d_x d_y} = \frac{|\hat{G}_{d_x d_y}|^2}{\hat{G}_{d_x d_x}\hat{G}_{d_y d_y}} \tag{17}$$

Partial coherence functions provide estimates of the

linear relationships between one input (D_x or D_y) and one output (X_x or X_y) and is given by (Bendat and Piersol, 1986):

$$\hat{\gamma}^2_{d_i x_j \cdot d_k} = \frac{|\hat{G}_{d_i x_j \cdot d_k}|^2}{\hat{G}_{d_i d_j \cdot d_k} \hat{G}_{x_i x_j \cdot d_k}} \quad i, j, k \in [1, 2], \quad i \neq k \tag{18}$$

where the residual spectra $\hat{G}_{d_i x_j \cdot d_k}$ are defined as:

$$\hat{G}_{d_i x_j \cdot d_k} = \hat{G}_{d_i x_j} \left[1 - \frac{\hat{G}_{d_i d_k} \hat{G}_{d_k x_j}}{\hat{G}_{d_k d_k} \hat{G}_{d_i x_j}} \right] \tag{19}$$

Working out the substitution of Eq. (19) into Eq. (18) gives:

$$\hat{\gamma}^2_{d_i x_j \cdot d_k} = \frac{|\hat{G}_{d_i x_j} \hat{G}_{d_k d_k} - \hat{G}_{d_k x_j} \hat{G}_{d_i d_k}|^2}{\hat{G}^2_{d_k d_k} \hat{G}_{d_i d_i} \hat{G}_{x_j x_j} (1 - \hat{\gamma}^2_{d_k d_i})(1 - \hat{\gamma}^2_{d_k x_j})} \tag{20}$$

with $\hat{\gamma}^2_{d_k d_i}$ the ordinary coherence function between both inputs, defined by Eq. (17), and $\hat{\gamma}^2_{d_k x_j}$ the ordinary coherence function between one input and one output and defined as:

$$\hat{\gamma}^2_{d_k x_j} = \frac{|\hat{G}_{d_k x_j}|^2}{\hat{G}_{d_k d_k} \hat{G}_{x_j x_j}} \tag{21}$$

Partial coherence functions are equivalent to ordinary coherence functions after the effects of all other inputs have been removed from both input and output of interest (Bendat and Piersol, 1986). Because the input coherence (Eq. (17)) is part of their expressions, multiple and partial coherence functions compensate for coupling between the input signals.

2.3. A particular case: the open-loop estimator

Normally, the arm is interacting with an environment and it was argued that a closed-loop estimator was necessary to obtain an estimate of the arm compliance. A typical application of open-loop estimators accounts in the case position disturbances are applied using a strong servo controlled manipulator that simply imposes (or dictates) a prespecified movement irrespective of the generated hand force. The corresponding open-loop estimator, as used by Perreault et al. (1999), can be derived from the closed-loop estimator in the following way. Let the environment be dominant over the arm, i.e. $E_{xz} \ll H_{xf}$ or $E_{xz} \to 0$, then $L \to I$.

Additionally, let the external force disturbance increase proportionally such that $\mathbf{D} \gg \mathbf{F}$. Now, Eqs. (5) and (6) become:

$$\mathbf{F}^T = \mathbf{D}^T E_{xz}^T H_{xf}^{-1^T} + \mathbf{N}^T$$

$$\mathbf{X}^T = \mathbf{D}^T E_{xz}^T + \mathbf{M}^T$$

The product $\mathbf{D}^T E_{xz}^T$ actually describes the imposed position disturbance. Taking $\mathbf{D}^T E_{xz}^T = \mathbf{X}_{\text{dist}}^T$ as the position disturbance, and substituting it into the above equations gives:

$$\mathbf{F}^T = \mathbf{X}_{\text{dist}}^T H_{xf}^{-1^T} + \mathbf{N}^T$$

$$\mathbf{X}^T = \mathbf{X}_{\text{dist}}^T + \mathbf{M}^T$$

Effectively, $\mathbf{X}_{\text{dist}}$ has become the exciting input of the arm and this is true as long as $\mathbf{X} = \mathbf{X}_{\text{dist}}$ (assuming $\mathbf{M} \ll \mathbf{X}_{\text{dist}}$). Evidently, the hand reaction force $\mathbf{F}$ must be taken as the responding output. Assuming that both noise sources are uncorrelated with the input $\mathbf{X}_{\text{dist}}$, the open-loop estimator becomes:

$$\hat{G}_{xx}^{-1} \hat{G}_{xf} = \hat{H}_{xf}^{-1^T}$$

For correctness of terms, in the above equation the arm impedance (inverse of compliance) is given because the force is assumed as an output. Accordingly, the coherences functions need to be expressed between $\mathbf{X}$ and $\mathbf{F}$.

The other situation for which an open-loop estimator can be derived is the ideal case that the manipulator has no dynamics. This means that $E_{xz} \to \infty$ and similar steps can easily be followed to arrive at an open-loop estimator for the arm compliance. In that case, $\mathbf{F}$ is the exciting input and is equal to $\mathbf{D}$.

2.4. Variance and bias of spectral density estimators

The goodness of the estimation is judged by the bias and variance of the applied estimator. Variance is the result of random parts in the signals and is reduced by averaging the raw spectra ($\hat{G}_{df}$ and $\hat{G}_{dx}$) over m adjacent frequencies (Jenkins and Watts, 1968). As the result, the frequency resolution decreases to $m\Delta f$ such that the estimated compliance is defined at the following frequencies:

$$\hat{H}_{xf}(n\Delta f) \overset{\text{aver.}}{\to} \hat{H}_{xf}(\Delta f_1 + pm\Delta f) \quad p \in \left[1, 2, \ldots, \frac{N-m}{m} \right]$$

with Δf_1 the lowest frequency after averaging according to:

$$\Delta f_1 = \frac{1}{m} \sum_{n=m+1}^{n=2m} n\Delta f$$

From the above equation it can be seen that the zeroth frequency is removed from the spectral densities (related to the mean values of the signals) by omitting the first averaging window.

To preserve a certain minimal frequency resolution in order not to average out peaks in the (M)FRFs, m should be limited. Alternatively, the record time can be increased, albeit restrictively to avoid fatigue effects during experiments with humans in vivo.

Bias is the result of structural differences between the estimated value and the real value. The largest bias contribution is caused by the finiteness of the time

records (Bendat and Piersol, 1986; Perreault et al., 1999). In the case of long observations and a large number of averaging frequencies, the bias of the spectral densities approaches zero (Jenkins and Watts, 1968).

Variance of the estimated MFRFs is also reflected by variance of the multiple coherence functions and bias results in a decrease of the multiple coherence (Bendat and Piersol, 1986; Perreault et al., 1999). Therefore, multiple coherence functions will be taken as the explicit indicators for the robustness of the estimator.

In addition to noise, the disturbance signal also enters the system. In many studies this signal has been taken to be stochastic too (Kirsch et al., 1993; Cathers et al., 1999; Perreault et al., 1999, 2001), leading to a further increment of bias and variance (Schoukens et al., 1993). This is because the spectral properties of stochastic signals are captured only from infinitely long observations and defined on a continuous frequency scale, while for a finite observation time the system can only be defined at discrete frequencies $n\Delta f$. To exclude this negative effect, a specific signal design method has been adopted which is described in the following section.

2.5. Disturbance signal design

The disturbance signal will be designed in the frequency domain such that the signal is completely determined within T seconds in order to avoid bias. Any spectrum can be realized, resulting in a sum of sine waves with different frequencies. Using these multisine signals (Schoukens et al., 1993), the system is identified at those frequencies ($n\Delta f$) constituting the disturbance signal. To make the signal unpredictable for subjects, the phases between all frequency components are randomized.

The structure of the Fourier transform $\mathbf{\Psi}(n\Delta f)$, of the time signal $\psi(l\Delta t)$ to be constructed, is determined as follows:

$$\begin{aligned}\mathbf{\Psi}(n\Delta f) &= \sum_{n=1}^{N/2} \mathbf{\Lambda}(n\Delta f)e^{j\mathbf{\Theta}(n\Delta f)} \\ &= \lambda_1(\cos\,\theta_1 + j\,\sin\,\theta_1) + \ldots \\ &\quad + \lambda_{N/2}(\cos\,\theta_{N/2} + j\,\sin\,\theta_{N/2})\end{aligned} \tag{22}$$

with $\mathbf{\Theta}(n\Delta f)$ a sequence of randomly generated phases in the range $[0\ldots 2\pi]$:

$$\mathbf{\Theta}(n\Delta f) = [\theta_1 \ldots \theta_{N/2}] \tag{23}$$

and $\mathbf{\Lambda}(n\Delta f)$ a sequence of vector magnitudes:

$$\mathbf{\Lambda}(n\Delta f) = [\lambda_1 \ldots \lambda_{N/2}]$$

The amplitude of each sine wave λ_n is adjusted to obtain the appropriate spectral power distribution. For the random generation of the phases, any type of distribution will suffice. In this case, a uniform distribution is applied. Applying the inverse fast Fourier transform (IFFT) to the N-point frequency vector $[\mathbf{\Psi}(-n\Delta f)\mathbf{\Psi}(0)\mathbf{\Psi}(n\Delta f)]$ directly gives the corresponding time signal $\psi(l\Delta t)$, with $l = 1\ldots N$.

3. Simulations

The accuracy of the estimator of the dynamic arm compliance (Eq. (13)) is analyzed for different controlled conditions. For this purpose, computer simulations are performed for varying properties of:

- the compliance of the arm,
- the compliance of the environment,
- input and output noise,
- the number of averaging frequencies,
- the length of the observation time.

3.1. Arm–environment model

If both arm and environment were coupled mass-damper-spring systems, the hand reaction force $\mathbf{F}(t)$ would not be observable, i.e. could not be a system output. This is because force is also a function of the second derivative while only the zeroth (positions) and first derivatives (velocities) are part of the state space. To obtain the hand reaction force, handgrip visco-elasticity is incorporated into the model, which represents the dynamics between the arm and the environment. In fact, the handgrip visco-elasticity decouples the mass of both arm and environment such that the hand reaction force is determined by the difference in velocity and position between both masses. A representation of

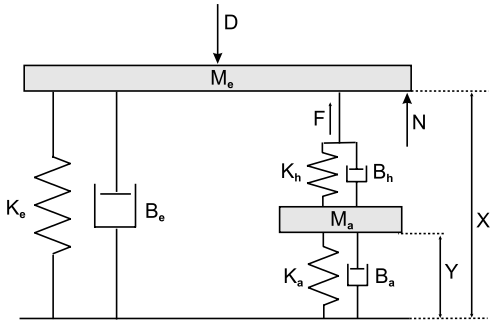

Fig. 4. Model representation of the mechanical compliance of the arm and the environment as used for simulation. The representation is merely to illustrate the model equations and is simply reduced here to one degree of freedom. M_e, B_e, K_e represent the mass-damper-spring system of the environment. B_h, K_h represent the visco-elasticity of the handgrip and M_a, B_a, K_a represent the mass-damper-spring system of the arm. **D** is the external force disturbance acting upon the whole system. **Y** is the arm position and **X** the position of the endpoint or hand. **F** is the hand reaction force and **N** is the input noise from uncorrelated activation of the muscles. Note that both masses are decoupled by the handgrip visco-elasticity.

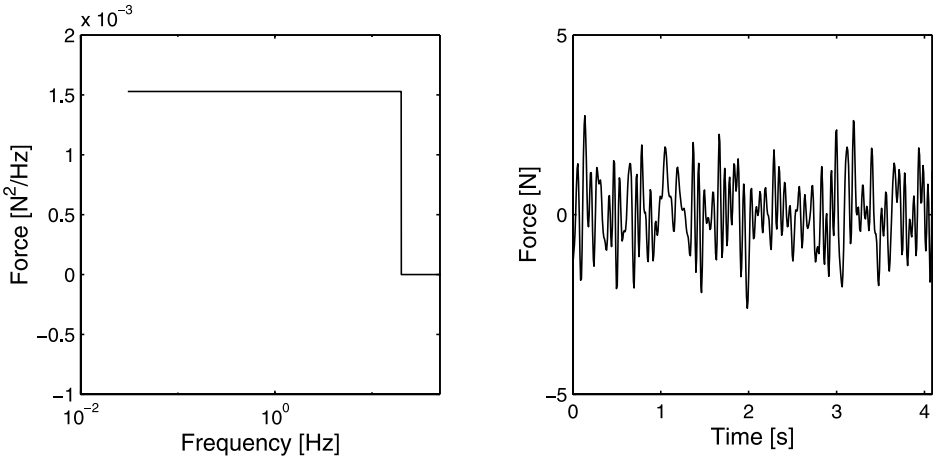

Fig. 5. Realization of an input disturbance signal. Left, power spectral density. Right, corresponding time signal (only the first 4 s). Standard deviation: 1 N.

the complete system of arm and environmental compliance is given in Fig. 4. The representation is simplified to one degree-of-freedom (for the drawing only) and taken to be linear. A linear approximation of the planar endpoint dynamics is justified for small amplitude displacements (Dolan et al., 1993; Acosta et al., 2000).

The model is described in state-space form (Appendix A). The state vector is:

$$\mathbf{X} = [\dot{X}\, X\, \dot{Y}\, Y]^T$$

with X and Y the position and $\dot{X}$ and $\dot{Y}$ the velocity of the hand and arm, respectively. The inputs are $\mathbf{D}(t)$ and $\mathbf{N}(t)$, and the outputs are $\mathbf{X}(t)$ and $\mathbf{F}(t)$. The output noise $\mathbf{M}(t)$ is added to the model output $\mathbf{X}(t)$. Fig. 5 shows an example of an input signal that is used for simulation. The lowest frequency in this signal was approximately 0.03 Hz ($=1/T$ for $T=32.768$) and the highest approximately 20 Hz, which is a sufficient bandwidth to capture all arm dynamics (Perreault et al., 2001). The signals are scaled such that the standard deviation is 1 N.

Model simulations were performed in MATLAB/SIMULINK® (The MathWorks, Inc.) using a variable time step Runge–Kutta (Dormand–Prince) solver. The resulting signals were linearly interpolated to obtain equidistant time samples at 125 Hz ($N=2^{12}$ samples for $T=32.768$ s) reconstruction frequency (zero order hold).

3.2. Model parameters

Two typical sets of arm-model parameters were taken from the experiments of Tsuji et al. (1995), given in Table 1. To evaluate the effect in the case where the arm compliance contains a high resonance peak, a third parameter set is used containing a reduced arm damping of 25% of the default value (see Table 1). The default parameter set is indicated with an asterisk.

The visco-elastic handgrip parameters were taken from recent experiments from our group (De Vlugt et al., 2002):

Table 1
Parameters of the dynamic compliance of the arm (set 1 and 2), adopted from Tsuji et al. (1995) (their Table 4, subject A, position 1 and 2, respectively)

	M_a [kg]		B_a [N s/m]		K_a [N/m]	
1*	1.22	−0.31	12.2	−9.68	131	−123
	−0.28	0.57	−10.1	16.9	−141	283
2	0.96	−0.57	5.03	−4.13	58.3	−45.6
	−0.55	0.98	−3.99	30.0	−54.0	506
3	1.22	−0.31	3.05	−2.42	131	−123
	−0.28	0.57	−2.53	4.23	−141	283

M_a, mass matrix; B_a, damping matrix and K_a, stiffness matrix. The third parameter set contains a value for damping which is 25% of that of the first parameter set while the mass and stiffness were taken as equal. Asterisk indicates the default parameter set.

Table 2
Parameters of the environment used for simulation, with M_e, mass matrix; B_e, damping matrix and K_e, stiffness matrix

	M_e [kg]		B_e [N s/m]		K_e [N/m]	
1*	1	0	0	0	0	0
	0	1	0	0	0	0
2	2.53	0	223	0	10000	0
	0	2.53	0	223	0	10000

The first combination represents a high environmental compliance and is used for the application of force disturbances. The second combination represents a low compliance having a flat bandwidth of 10 Hz, typically used for position disturbances. Asterisk indicates the default parameter set.

$$B_h = \begin{bmatrix} 200 & 0 \\ 0 & 200 \end{bmatrix} \text{ [N s/m]},$$

$$K_h = \begin{bmatrix} 15\,000 & 0 \\ 0 & 15\,000 \end{bmatrix} \text{ [N/m]}$$

with B_h, the grip viscosity and K_h the grip elasticity matrix. These parameter values were taken the same for all simulations.

Table 2 gives the parameter sets of two extreme environments. The first set (default) corresponds to a high compliance, appropriate for the application of force disturbances. A symmetric endpoint mass of 1 kg is taken which, in our experience, is a minimum for a typical two-linkage manipulator. The second parameter set represents a very low compliance, typically that of a position controlled (stiff) manipulator and appropriate for the application of position disturbances. This parameter set was chosen such that the MFRF is flat (critically damped) having a bandwidth of 10 Hz.

The power of the noise contribution is expressed as the signal-to-noise ratio (SNR) in decibels [dB]:

$$\text{SNR} = 10^{10} \log\left(\frac{G_{nn}}{G_{dd}}\right) \text{ [dB]} \tag{24}$$

with G_{nn} the power spectrum of the input noise, and G_{dd} the power spectrum of the disturbance signal. In case of output noise: G_{nn} is replaced by G_{mm} and G_{dd} by G_{xx}.

3.3. Methodological parameters

The accuracy of the estimator is judged for different values of noise levels, observation time period and width of the frequency window used for averaging. The values are given in Table 3 where the defaults are indicated with an asterisk. The most meaningful combinations of these different parameter values are evaluated and the results are described in the following section.

Table 3
Estimator and simulation parameters

SNR_f, SNR_x (dB)	T (s)	m (–)
−20*	32.768*	4*
−10	16.384	8
0	8.192	16

SNR_f and SNR_x, signal to noise ratios for input and output noise, respectively; T, observation time length; m, number of averaging frequencies. Asterisk indicates the default parameter set.

4. Results

4.1. Arm compliance

Fig. 6 shows the estimated dynamic compliance $H_{xf}(n\Delta f)$ for parameter sets 1 and 2 of Table 1. All other parameters were set at their default values. For almost all frequencies, the estimated MFRFs are very good approximations of the modeled MFRFs (dotted lines). Any deviation from the modeled compliance is the result of noise and the application of frequency averaging that increase the variance and bias. For the off-diagonal elements, the estimates deviate the most. Especially for parameter set 2 where the off-diagonal elements of the compliance were smallest (less contribution to the output) such that the SNR was highest. The accuracy of the compliance estimates is reflected by the coherence functions shown in Fig. 7. For the diagonal elements, the output is almost linearly related to the input for all frequencies as indicated by high values of the corresponding partial coherence functions. The deviations of the estimated compliance for the off-diagonal elements are reflected by smaller values of the partial coherence functions. The multiple coherence functions are high for all frequencies, indicating a predominant linear behavior between force disturbance and hand position.

Hereafter, only the multiple coherence functions will be shown for convenience of comparison.

4.2. Environmental compliance

For high compliance of the environment, the multiple coherence is mainly determined by the arm compliance. In the case where the compliance of the environment is severely lowered (second parameter set, Table 2) the overall system MFRF will mainly be determined by the compliance of the environment. Consequently, any bias around the resonance frequency of the arm, due to averaging out its resonance peak, will vanish. For a clear illustration of this effect, the highly resonant arm compliance (third parameter set in Table 1) is used for both types of environments. The increase of the multiple coherence functions is clearly demonstrated as being due to the dominance of the environment (Fig. 8, from solid lines to dotted lines).

4.3. Input and output noise

Both noise signals are generated as a stochastic sequence of time samples and filtered at 20 Hz (fourth order Butterworth) to avoid aliasing. With increasing power level of both input and output noise, the estimated multiple coherence functions decrease, as was expected (Fig. 9). The coherence functions are still very high (>0.8) for SNRs of -10 dB. When the power

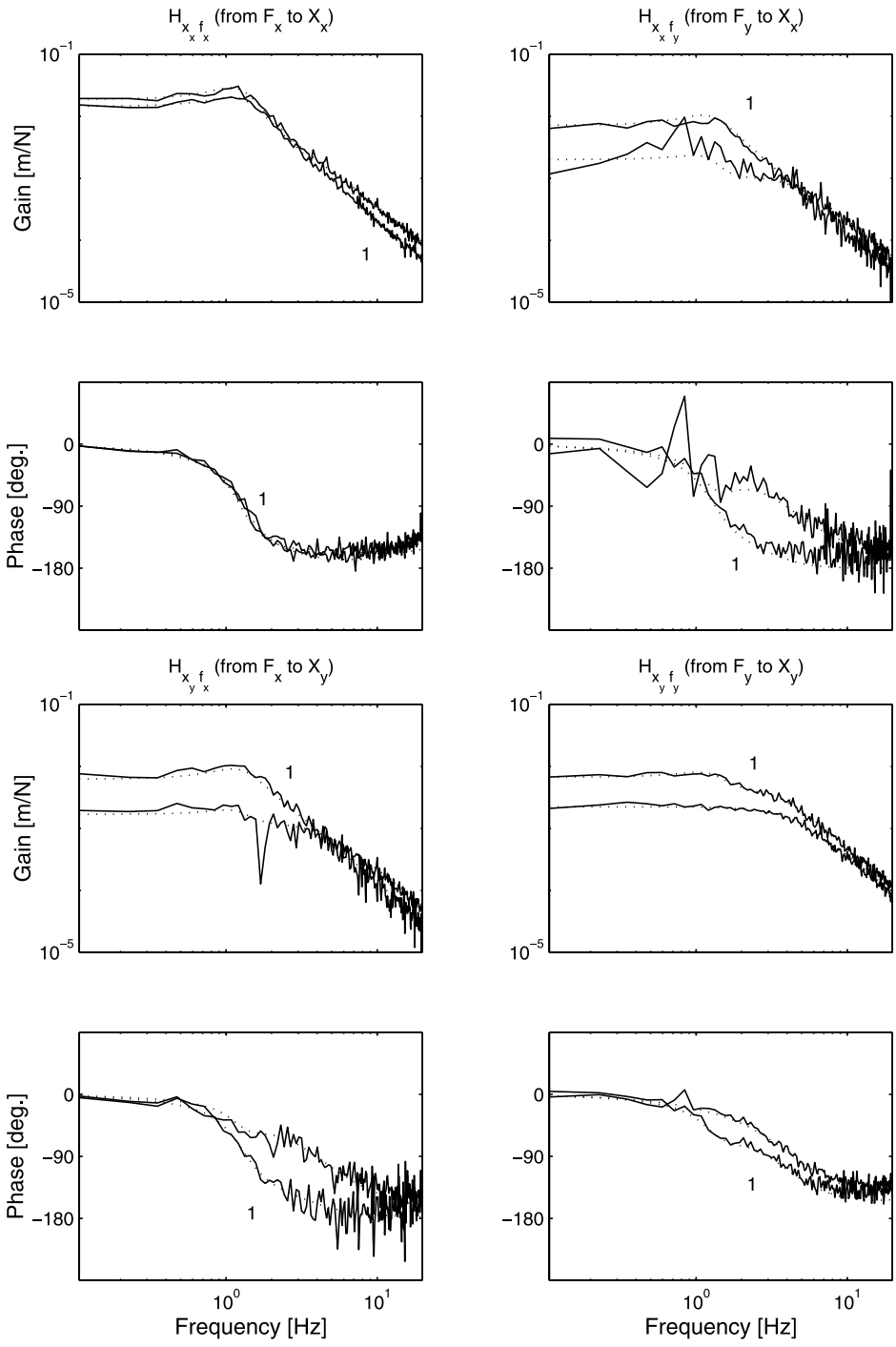

Fig. 6. Estimated dynamic compliance H_{xf} of the arm for parameter sets 1 and 2 (set 1 labeled by 1's). Solid lines, estimations; dotted lines, model. All other parameters are set at the default values.

of the noise is as large as that of the signal itself (SNR = 0 dB), the estimated multiple coherence functions remain mostly above 0.4.

4.4. Frequency averaging and observation time length

The smoothing effect of averaging is largest in the case of severe noise. For large stochastic noise power (SNR = 0 dB) at both input and output in combination with only four averaging frequencies ($m = 4$), variance and bias of the estimated coherence functions are large (Fig. 10). For $m = 16$, the variance is smaller resulting in smoother estimates of the coherences.

The effect of the observation time length is analyzed for the default conditions, except that no noise is applied. Then the only cause for bias is the width of

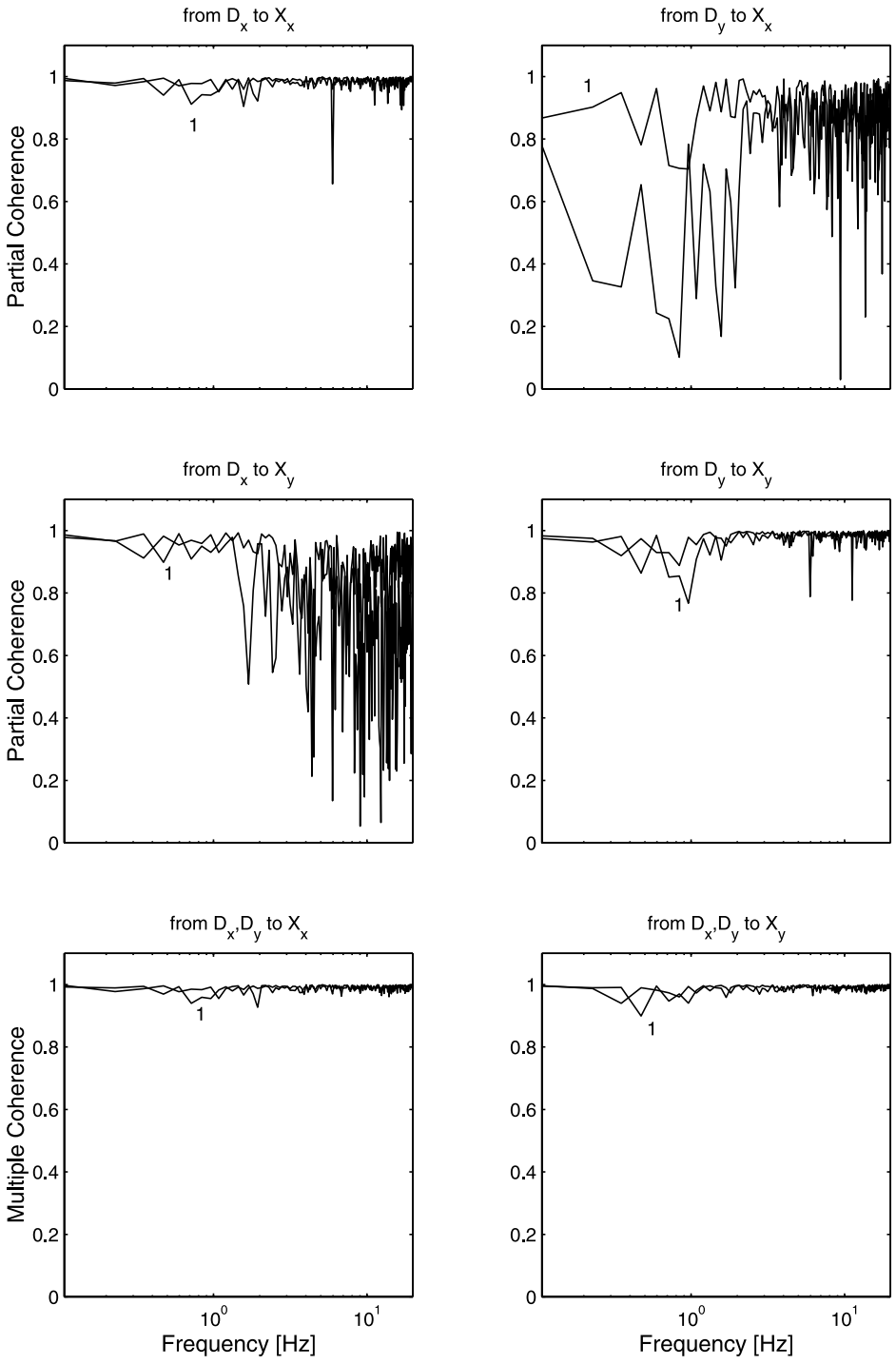

Fig. 7. Estimated coherence functions corresponding to the complete system from force disturbance D to end point position X corresponding to the estimates shown in Fig. 6 (parameter set one labeled by 1's). Upper two rows, partial coherence functions; bottom row, multiple coherence functions.

the frequency window used for averaging, which is directly dependent on the number of averaging frequencies (m) and reciprocally on the observation time length (T). Fig. 11 shows the estimated multiple coherence functions for 32.768, 16.384 and 8.192 s ($m = 4$). The multiple coherence functions decrease to a minimum for the shortest record length at the eigenfrequency of the arm where the variation of the MFRFs is largest. For this short observation, the width of the frequency window was largest, i.e. $m/T = 4/8.192 \approx 0.5$ Hz. The multiple coherence was still very high (> 0.8, Fig. 11, upper row). For comparison, the same exercise is performed but now with different window widths to preserve the same frequency resolution. Therefore, $m =$

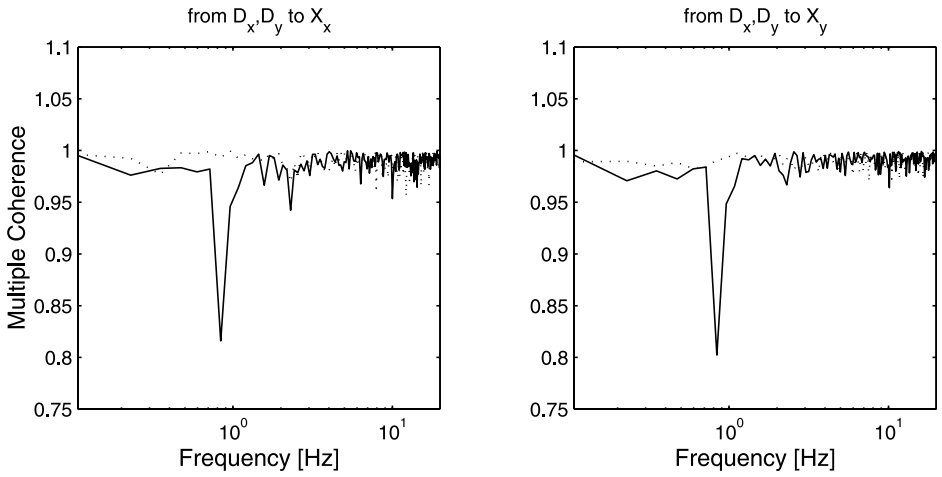

Fig. 8. Multiple coherence estimates in the case of different admittances of the environment. Arm damping B_a is set to 25% of its default value. Solid lines, large (default) compliance of the environment. Dashed dotted lines, low compliance of the environment. Note the lowest value on the ordinate is 0.75.

16, 8 and 4 for $T = 32.768$, 16.384 and 8.192 s, respectively. Fig. 11 (bottom row) now shows that all estimated multiple coherence functions exhibit a minimum, which is more or less the same.

5. Discussion

This article presents a new multivariable closed-loop identification method to estimate the compliance of the

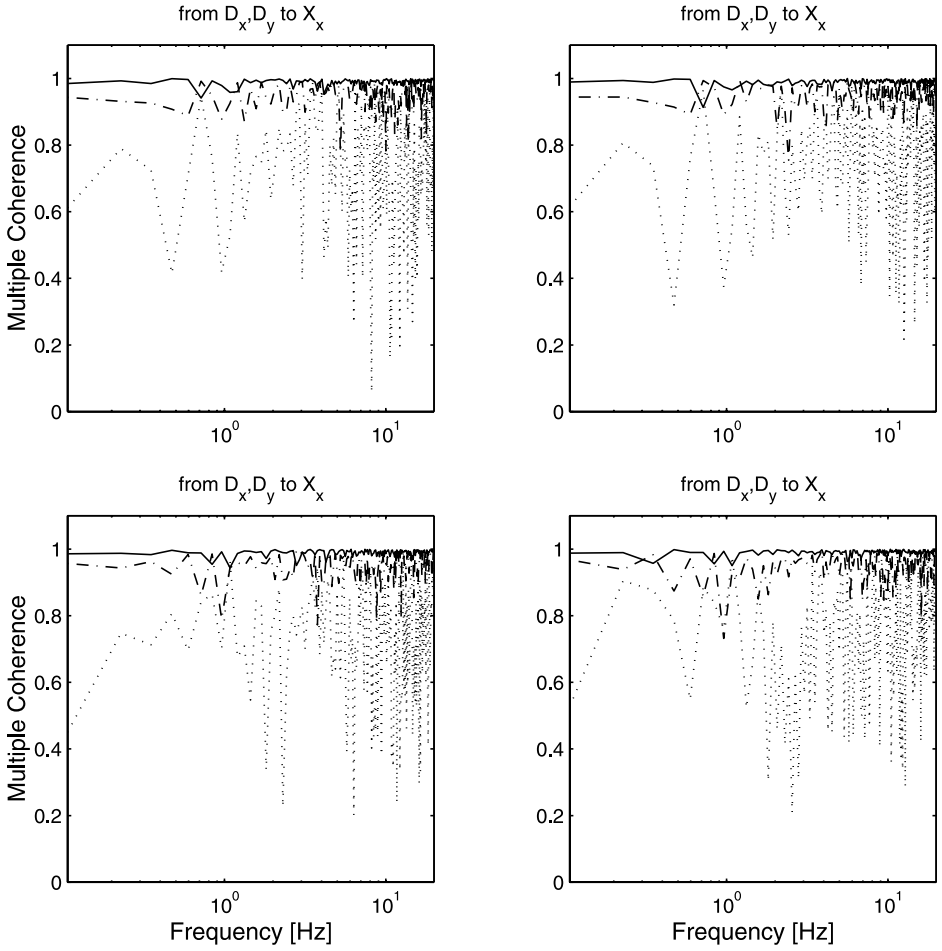

Fig. 9. Estimated multiple coherence functions for different signal-to-noise ratios at the input (upper row) and output (bottom row): −20 dB (solid lines); −10 dB (dashed-dotted lines) and 0 dB (dotted lines).

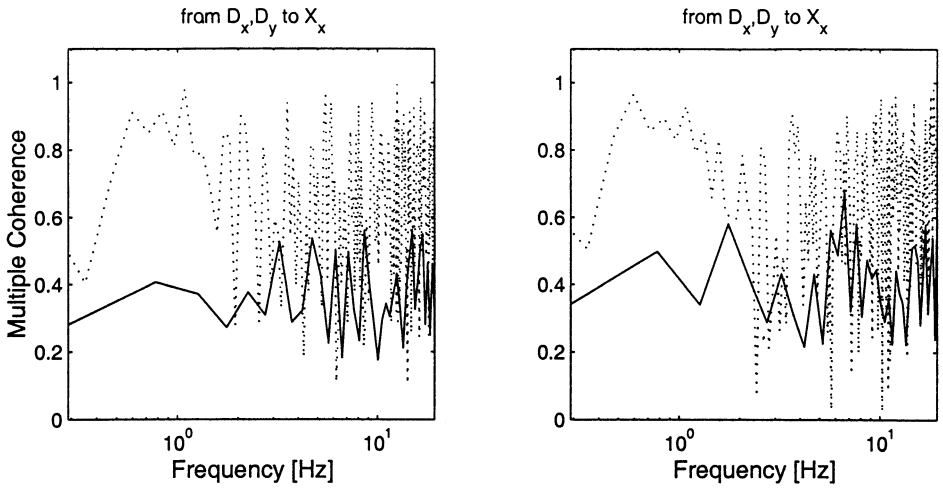

Fig. 10. Estimated multiple coherence functions for two different numbers of averaging frequencies (m) in case of large noise power at both input and output (SNR = 0 dB). $m = 4$ (dotted lines), $m = 16$ (solid lines).

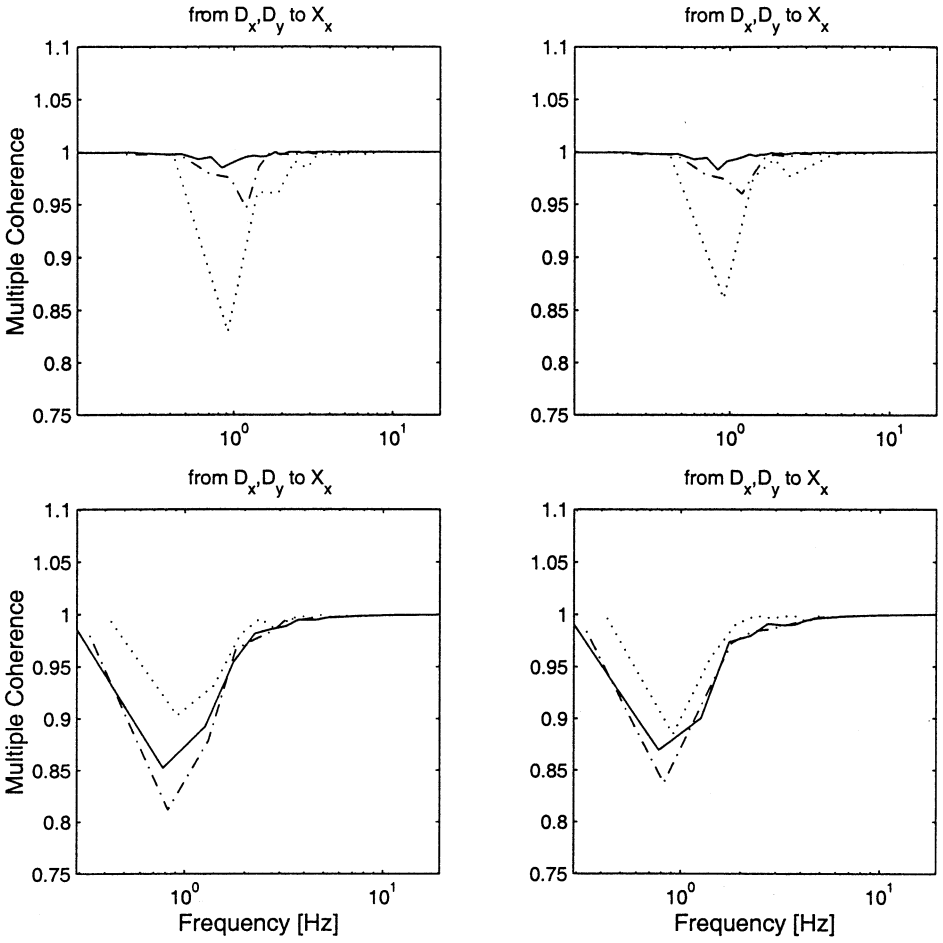

Fig. 11. Estimated multiple coherence functions for different observation time lengths (upper row) without noise. $T = 32.768$ s (solid lines); $T = 16.384$ s (dashed–dotted lines) and $T = 8.192$ s (dotted line). Bottom row: $T = 32.768$ s with $m = 16$ (solid lines); $T = 16.384$ s with $m = 8$ (dashed–dotted lines) and $T = 8.192$ s with $m = 4$ (dotted line). Note the lowest value on the ordinate is 0.75.

arm during excitation with continuous force disturbances. The method is applicable to posture tasks where interaction with an environment takes place, which always results from the application of force disturbances. The accuracy of the estimator is tested for different parameters of the dynamic compliance of the arm and several methodological conditions.

In the following, the performance and limitations of the estimator, the validity of the arm model, the properties of the disturbance signals and the relevance of applying force disturbances are discussed.

5.1. Estimator performance

Estimates are always contaminated with bias (structural errors) and variance (random errors). Both are primarily the result of noise. Input noise comes from additional inputs that are uncorrelated with the force disturbance signal, like uncorrelated muscle activation, and can be minimized by preventing anticipatory behavior of the subject. To rule out anticipation, unpredictable (random) disturbances are necessary. Output noise is mainly caused by system nonlinearities and time variant behavior of the limb and environment. Nonlinearities can be minimized using small amplitude disturbances and application of high performance (linear) manipulators. Time variant behavior is likely to be minimal with clear and natural task instructions that are translated by the CNS into unambiguous motion control actions.

For modeling purposes, noise at the input can easily be replaced by noise at the output, accounting for the difference of the MFRF of the combined system. The input noise power was almost constant over frequency while the power of the output noise was taken as a scaled version of the output itself, according to the expression of the SNR (Eq. (24)). Hence, the difference between the input and output noise power is determined (approximately) by the gain of the MFRF of the combined system such that their net effects are the same at the output (Fig. 9). Despite this rather simplistic combination of input and output noise power, it clearly demonstrates that high frequency input noise deteriorates the estimates to a lesser extent than high frequency output noise. This is due to the filtering effect of the system compliance.

Averaging of the raw spectra over adjacent frequencies is applied, which effectively reduces the variance (Fig. 10). Another positive effect of averaging is that bias in the estimates of the partial and multiple coherence functions decreases (Jenkins and Watts, 1968). This is also clear from Fig. 10 where the estimates are apparently too high for $m = 4$ compared with those for $m = 16$. The disadvantage of frequency averaging is the increase of bias due to the decrease of the frequency resolution. Bias is particularly large at frequencies where the MFRF of the system to be identified contains abrupt changes, e.g. from oscillatory behavior (Fig. 8). The trade-off between the positive and negative effects of frequency averaging can primarily be solved with increasing the observation time length (Fig. 11).

Another source of bias and variance originate from the application of stochastic disturbance signals (Schoukens et al., 1993). The bias can be reduced by substantially increasing the observation time length, as mentioned before. However, to avoid time variant behavior due to fatigue in the case of in vivo experiments, long observations are undesirable. Application of deterministic disturbances, like the multisine signals in this study, instead of stochastic noise has been proved to reduce bias in the estimates (Peeters et al., 2001).

An important property of the estimator is the accurateness for short observations. For instance, a 8.192 s observation time length and only four averaging frequencies still results in high multiple coherence functions (> 0.8, Fig. 11), at a frequency resolution of $\Delta f = 4/8.192 \approx 0.5$ Hz.

An alternative averaging method, as used in the study by Perreault et al. (1999), is the periodogram approach or Welch method (Welch, 1967). This method relies on segmentation in the time domain of the measured signals and performing spectral estimates on each segment. The raw estimates of each periodogram are averaged and used to calculate the final estimate of the arm compliance, using the same estimator as used in this study. The Welch method is, therefore, less suitable to deterministic signals as used in this study because the requirement was that the observation time length should be the same as the period of the disturbance signal in order to achieve the exclusion of bias. Because segmentation introduces bias, a deterministic disturbance is not preferred anymore to a stochastic one for application of the Welch method. Hence, the advantage of deterministic signals does not apply to the Welch method.

For the same model parameters and noise power, Perreault et al. (1999) showed values of the estimated multiple coherences of about 0.7 with a 2.56 s (Welch) window ($\Delta f = 1/2.56 \approx 0.4$ Hz). Our results showed somewhat higher values (> 0.8, Fig. 11) for a comparable frequency resolution ($T = 8.192$, $m = 4$, $\Delta f \approx 0.5$). Similarly, for higher frequency resolutions, i.e. $T =$ 16.384 and 32.768 s in our case (with a constant number of averaging frequencies of $m = 4$) against Welch-window sizes of 5.12 and 10.24 s, respectively, the estimates of the multiple coherences are comparable. However, their results required a total observation time length of 60 s, which is more than seven times longer than in our case for $T = 8.192$, and four times and two times longer in the case of $T = 16.384$ and 32.768 s, respectively. Generally, the identification method presented here requires relatively short observations and moderate averaging to preserve sufficient frequency

resolution with reasonably high values of the multiple coherence functions. It is proved by this study that the current identification method together with the application of the deterministic disturbances offers accurate estimations, within observation times that are substantially shorter than required by the Welch method. Evidently, experiments should be conducted to verify high multiple coherences during such a short observation times in practice.

Perreault et al. (1999) used a sampling frequency of 50 Hz against 125 Hz in this study. However, sampling frequency has no influence on the frequency resolution and, therefore, does not change the results. The advantage of a higher sampling rate is that low-pass anti-aliasing filters can be applied with cut-off frequencies sufficiently above the frequency range of interest, which is approximately 20 Hz for mechanical properties of the arm.

Coherence functions apply to independent inputs and the outputs of the combined closed-loop system. In the case where the compliance of the environment is substantially lower than that of the arm, the estimated multiple coherence function is largely determined by the (linear) environment instead of the arm (Fig. 8). An open-loop estimator should be used in these cases to circumvent this problem. However, in the case of force disturbances, a high environmental compliance is primarily desired resulting in an input–output behavior that is mainly determined by the arm compliance. In these cases, coherence functions, therefore, are largely determined by the arm compliance.

5.2. Frequency versus time domain identification

An alternative to the frequency domain is identification in the time domain. The corresponding nonparametric time domain identification then provides estimates of the system's matrix impulse response function (MIRF). For linear open-loop systems, both time and frequency domain identification obtain comparable estimates (Perreault et al., 1999). Besides numerical differences, there is a preference for MFRFs to MIRFs with respect to visual presentation. Where MIRFs are poor indicators of the system dynamics and give only insight in the time extent or memory of the system, MFRFs show important global properties of dynamic systems such as the order of the system, relative damping and regions of oscillatory behavior.

Apart from these general differences, a detailed comparison cannot be made because nonparametric identification in the time domain has not been studied previously for closed-loop systems. Usually, parametric estimators in the time domain are applied using a fixed model structure of the system to be estimated. Parametric identification is less attractive in the first stage when detailed knowledge of the system structure is not at hand. A proofed method to quantify the parameters of a single-joint arm model is the application of a nonparametric estimator in the first stage, followed by (least squares) fitting of a parametric model onto the estimates as the second stage (Van der Helm et al., 2002).

5.3. Validity of the arm model

The arm model used is very simple, only consisting of a linear mass-damper-spring system. This model is frequently used to describe the input–output behavior of limbs at endpoint (mostly the hand) for small continuous displacements around a reference point under different experimental conditions (Dolan et al., 1993; Tsuji et al., 1995; Gomi and Kawato, 1996; Gomi and Osu, 1998; Perreault et al., 2000, 2001). Despite its limited descriptive ability, since it is only a lumped representation of intrinsic and reflexive dynamics together, these studies showed that this model is quite accurate for the conditions studied. In previous studies from our group, we extended the mass-damper-spring system with linear position and velocity feedback to separately identify the gains of muscle spindles (De Vlugt et al., 2002; Van der Helm et al., 2002). For the experimental conditions applied, we found that both gains depend on the frequency content of the force disturbance and damping of the environment. Despite the highly nonlinear behavior of the muscle spindles, mainly due to their unidirectional sensitivity to stretch (Kirsch et al., 1994; Stein and Kearney, 1995; Kearney et al., 1997; Zhang and Rymer, 1997; Mirbagheri et al., 2000), high values for the variance accounted for (VAF) were found with the linear endpoint model.

Other nonlinearities on the muscle level are the different calcium activation–deactivation rates, and mechanical properties of the contractile elements like the force–length and force–velocity characteristics (Winters and Stark, 1985). Apparently, in multiple muscle systems these nonlinearities cancel out at endpoint level under specific conditions. Application of the linear identification method as developed in this study seems, therefore, justified. Summarized: (1) the application of small amplitude disturbances simply do not excite appreciable nonlinearities; (2) unidirectional presumably turns into bidirectional behavior in the case of muscles acting as antagonistic pairs and (3) from a functional anatomical point of view, different muscles likely act at different lengths hence distributing their characteristics over a wider range of motion which smoothes out the nonlinearities.

5.4. Relevance of force disturbances

Application of force disturbances while performing a position task offers insight into the disturbance rejecting

behavior of the human controller, i.e. the properties of the arm compliance. This experimental condition equates to natural posture tasks that aim to minimize deviations around a fixed desired position. Examples are holding a steering wheel or positioning a drilling machine (in the lateral direction). The magnitude of positional deviations is dependent on the total compliance at the endpoint (hand) and evidently from the power of the disturbance. The total compliance is the sum of the compliance of the arm and the environment, i.e. the dynamic compliance of the steering wheel in this example. Because there is mutual interaction, the endpoint compliance can be adapted through changing the compliance of the human arm.

The advantage of continuous disturbances is that subjects have the opportunity to adapt to the disturbance, in contrast to transient disturbances. In particular for unpredictable continuous disturbances, the arm compliance can only be changed by different (constant) levels of intrinsic and reflexive contributions. In general, high (co)contraction and large feedback from muscle spindles can potentially decrease the arm compliance and hence improve the disturbance rejection.

Simulation studies have shown that intrinsic and reflexive mechanisms were effective for continuous unpredictable force disturbances where the task was to minimize hand displacements. In particular, high afferent position feedback was predicted for small bandwidth force disturbances (De Vlugt et al., 2001; Schouten et al., 2001). These results were very similar to a comparable experimental study by Van der Helm et al. (2002), and were explained from an optimal controller perspective, i.e. adjustment of the dynamic arm compliance to minimize displacements of the hand. Such explanations are only possible if the system is being perturbed by force disturbances such that all compliance mediating mechanisms have direct effect on the task performance (or hand displacement).

In the case of continuous position disturbances a force task seems logical (compared with force disturbances and a position task) and one is likely interested in mechanisms that are suited to control force, probably by Golgi tendon organs. Studies based on such an approach are not known to us. The challenge remains to clarify the role of different mechanisms, in particular reflexes that contribute to whole limb compliance for different tasks and during continuous disturbances. The degree of interaction and the type of disturbance signals are important aspects in (1) understanding the adaptability of the arm compliance by the CNS and (2) the choice (open or closed-loop) of the identification method. Unfortunately, these aspects were not fully recognized in the literature.

6. Conclusions

Closed-loop identification is necessary to estimate the mechanical properties of the arm using force disturbances where interaction with the environment always exists. This study proposes a new frequency-domain estimator that estimates the arm compliance from the closed-loop. The major advantages of the estimator are summarized below.

- The estimator is nonparametric such that no a priori system knowledge is required.
- The estimator is very accurate and requires only short observations periods.
- The application of deterministic multisine disturbance signals do not introduce bias and variance, and facilitates full control of the input spectra.

To understand the functionality of mechanisms controlling the dynamic compliance of the arm during posture tasks, the application of force disturbances and manipulable environments is important because it establishes a natural experimental condition. In order to estimate the arm compliance under such conditions, a closed-loop identification method as described in this study is indispensable.

Appendix A: State space model of arm, hand and environment

The complete model is described by three equations (see Fig. 4).

The arm model:

$$\mathbf{F}(s) + \mathbf{N}(s) = M_a\ddot{\mathbf{Y}}(s) + B_h\dot{\mathbf{Y}}(s) + K_h\mathbf{Y}(s) \tag{25}$$

The hand model:

$$\mathbf{F}(s) = B_h(\dot{\mathbf{X}}(s) - \dot{\mathbf{Y}}(s)) + K_h(\mathbf{X}(s) - \mathbf{Y}(s)) \tag{26}$$

The environmental model:

$$\mathbf{D}(s) - \mathbf{F}(s) = M_e(s)\ddot{\mathbf{X}}(s) + B_e\dot{\mathbf{X}}(s) + K_e\mathbf{X}(s) \tag{27}$$

where s is the Laplace operator. Eliminating $\mathbf{F}(s)$ by substituting Eq. (26) into Eqs. (25) and (27), results in the following two system equations:

$$\ddot{\mathbf{X}} = M_e^{-1}[-(B_e + B_h)\dot{\mathbf{X}} - (K_e + K_h)\mathbf{X} + B_h\dot{\mathbf{Y}} + K_h\mathbf{Y} + \mathbf{D}]$$

$$\ddot{\mathbf{Y}} = M_a^{-1}[B_h\dot{\mathbf{X}} + K_h\mathbf{X} - (B_h + B_a)\dot{\mathbf{Y}} - (K_h + K_a)\mathbf{Y} + \mathbf{N}]$$

where the Laplace operator is omitted for readability. The state space model equals:

$$\dot{\boldsymbol{\Psi}} = \mathbf{A}\boldsymbol{\Psi} + \mathbf{B}\mathbf{U}$$

$$\boldsymbol{\Phi} = \mathbf{C}\boldsymbol{\Psi} + \mathbf{D}\mathbf{U} \tag{28}$$

with $\mathbf{A}$ the 8×8 system matrix, $\mathbf{B}$ the 8×4 input matrix, $\mathbf{C}$ the 4×8 output matrix and $\mathbf{D}$ the 4×4 throughput

matrix:

$$\mathbf{A} = \begin{bmatrix} -M_e^{-1}(B_e + B_h) & -M_e^{-1}(K_e + K_h) & M_e^{-1}B_h & M_e^{-1}K_h \\ I & O & O & O \\ M_a^{-1}B_h & M_a^{-1}K_h & -M_a^{-1}(B_h + B_a) & -M_a^{-1}(K_h + K_a) \\ O & O & I & O \end{bmatrix}$$

$$\mathbf{B} = \begin{bmatrix} M_e^{-1} & O \\ O & O \\ O & M_a^{-1} \\ O & O \end{bmatrix}$$

$$\mathbf{C} = \begin{bmatrix} O & I & O & O \\ B_h & K_h & -B_h & -K_h \end{bmatrix}$$

$$\mathbf{D} = \begin{bmatrix} O & O \\ O & O \end{bmatrix}$$

$\mathbf{I}$ is the 2×2 identity matrix and $\mathbf{O}$ the 2×2 nulmatrix.

The state vector $\mathbf{X}$ equals:

$$\mathbf{\Psi} = \begin{bmatrix} \dot{\mathbf{X}} \\ \mathbf{X} \\ \dot{\mathbf{Y}} \\ \mathbf{Y} \end{bmatrix}$$

with $\mathbf{X} = [X_x X_y]$ and $\mathbf{Y} = [Y_x Y_y]^T$. The input and output vectors equal:

$$\mathbf{U} = \begin{bmatrix} \mathbf{D} \\ \mathbf{N} \end{bmatrix}$$

with $\mathbf{D} = [D_x D_y]^T$, $\mathbf{N} = [N_x N_y]^T$ and

$$\mathbf{\Phi} = \begin{bmatrix} \mathbf{X} \\ \mathbf{F} \end{bmatrix}$$

with $\mathbf{F} = [F_x F_y]^T$.

References

Acosta AM, Kirsch RF, Perreault EJ. A robotic manipulator for the characterization of two-dimensional dynamic stiffness using stochastic displacement disturbances. J Neurosci Methods 2000;102:177–86.

Bendat JS, Piersol AG. Random Data: Analysis and Measurement Procedures, 2nd ed. New York: Wiley, 1986.

Cathers I, O'Dwyer N, Neilson P. Dependence of stretch reflexes on amplitude and bandwidth of stretch in human wrist muscle. Exp Brain Res 1999;129:278–87.

De Vlugt E, van der Helm FCT, Schouten AC, Brouwn GG. Analysis of the reflexive feedback control loop during posture maintenance. Biol Cybern 2001;84:133–41.

De Vlugt E, Schouten AC, van der Helm FCT. Adaptation of reflexive feedback during arm posture to different environments. Biol Cybern 2002;87:10–26.

Doemges F, Rack PMH. Changes in the stretch reflex of the human first dorsal interosseous muscle during different tasks. J Physiol 1992a;447:563–73.

Doemges F, Rack PMH. Task-dependent changes in the response of human wrist joints to mechanical disturbance. J Physiol 1992b;447:575–85.

Dolan JM, Friedman MB, Nagurka ML. Dynamic and loaded impedance components in the maintenance of human arm posture. IEEE Trans Syst Man Cybern 1993;23:698–709.

Gomi H, Kawato M. Equilibrium-point control hypothesis examined by measured arm stiffness during multijoint movement. Science 1996;272:117–20.

Gomi H, Osu R. Task-dependence viscoelasticity of human multijoint arm and its spatial characteristics for interaction with environments. J Neurosci 1998;18(21):8965–78.

Hogan N. Impedance control: an approach to manipulation. Part I—theory. J Dyn Syst Meas Con 1985;107(1):1–7.

Jenkins GM, Watts DG. Spectral Analysis and its Applications. San Francisco: Holden Day, 1968.

Kearney RE, Hunter IW. System identification of human joint dynamics. CRC Crit Rev Biomed Eng 1990;18:55–87.

Kearney RE, Stein RB, Parameswaran L. Identification of intrinsic and reflex contributions to human ankle stiffness dynamics. IEEE Trans Biomed Eng 1997;44:493–504.

Kirsch RF, Kearney RE, MacNeil JB. Identification of time-varying dynamics of the human triceps surae stretch reflex. Exp Brain Res 1993;97:115–27.

Kirsch FK, Boskov D, Rymer WZ. Muscle stiffness during transient and continuous movements of cat muscle: disturbance characteristics and physiological relevance. IEEE Trans Biomed Eng 1994;41:758–70.

Ljung L. System Identification—Theory for the User, 2nd ed. Upper Saddle River, NJ: PTR Prentice Hall, 1999.

Milner TE, Cloutier C. Compensation for mechanically unstable loading in voluntary wrist movement. Exp Brain Res 1993;94:522–32.

Mirbagheri MM, Barbeau H, Kearney RE. Intrinsic and reflex contributions to human ankle stiffness: variation with activation level and position. Exp Brain Res 2000;135:423–36.

Mussa-Ivaldi FA, Hogan N, Bizzi E. Neural, mechanical, and geometric factors subserving arm posture in humans. J Neurosci 1985;5:2732–43.

Peeters F, Pintelon R, Schoukens J, Rolain Y. Identification of rotor-bearing systems in the frequency domain, Part I: estimation of frequency response functions. Mech Syst Signal Pr 2001;15(4):759–73.

Perreault EJ, Kirsch RF, Acosta AM. Multiple-input multiple-output system identification for characterization of limb stiffness dynamics. Biol Cybern 1999;80:327–37.

Perreault EJ, Crago PE, Kirsch RF. Estimation of intrinsic and reflex contributions to muscle dynamics: a modeling studyness dynamics. IEEE Trans Biomed Eng 2000;47:1413–21.

Perreault EJ, Kirsch RF, Crago PE. Effects of voluntary force generation on the elastic components of endpoint stiffness. Exp Brain Res 2001;141:312–23.

Schoukens J, Guillaume P, Pintelon R. Design of broadband excitation signals. In: Godfrey K, editor. Perturbation Signals for System Identification. Englewood Cliffs, NJ: Prentice-Hall, 1993:126–59.

Schouten AC, de Vlugt E, van der Helm FCT, Brouwn GG. Optimal posture control of a musculo-skeletal arm model. Biol Cybern 2001;84:143–52.

Smeets JB, Erkelens CJ. Dependence of autogenic and heterogenic stretch reflexes on pre-load activity in the human arm. J Physiol (Lond) 1991;440:455–65.

Stein RB, Kearney RE. Nonlinear behavior of muscle reflexes at the human ankle joint. J Neurophysiol 1995;73:65–72.

Toft E, Sinkjær T, Andreassen S, Larsen K. Mechanical and electromyographic responses to stretch of the human ankle extensors. J Neurophysiol 1991;65:1402–10.

Tsuji T, Morasso PG, Goto K, Ito K. Hand impedance characteristics during maintained posture. Biol Cybern 1995;72:475–85.

Van der Helm FCT, Schouten AC, de Vlugt E, Brouwn GG. Identification of intrinsic and reflexive components of human arm dynamics during postural control. J Neurosci Methods 2002;119:1–14.

Welch PD. The use of fast Fourier transform for the estimation of power spectra: a method based on time averaging over short, modified periodograms. IEEE Trans Audio Electroacoust 1967;15:70–3.

Winters JM, Stark L. Analysis of fundamental human movement patterns through the use of in-depth antagonistic muscle models. IEEE Trans Biomed Eng 1985;32:826–39.

Zhang LQ, Rymer WZ. Simultaneous and nonlinear identification of mechanical and reflex properties of human elbow joint muscles. IEEE Trans Biomed Eng 1997;44:1192–209.